Mathematical Biosciences 230 (2011) 1–11

Contents lists available at ScienceDirect

Mathematical Biosciences

journal homepage: www.elsevier.com/locate/mbs

A mathematical model of tumour and blood pHe regulation: The HCO_3^-/CO_2 buffering system

Natasha K. Martin [a,b,*], Eamonn A. Gaffney [a], Robert A. Gatenby [c], Robert J. Gillies [c], Ian F. Robey [d], Philip K. Maini [a,e]

[a] Centre for Mathematical Biology, Mathematical Institute, Oxford University, 24-29 St. Giles', Oxford, OX1 3LB, UK
[b] Department of Social Medicine, University of Bristol, Canynge Hall, 39 Whatley Road, Bristol, BS8 2PS, UK
[c] H. Lee Moffitt Cancer Center and Research Institute, 12902 Magnolia Drive, Tampa, FL 33612, USA
[d] University of Arizona, Tucson, AZ, USA
[e] Oxford Centre for Integrative Systems Biology, Department of Biochemistry, Oxford University, South Parks Road, OX1 3QU, UK

ARTICLE INFO

Article history:
Received 21 September 2010
Received in revised form 5 December 2010
Accepted 7 December 2010
Available online 15 December 2010

Keywords:
Buffering
Acidity
Cancer
Bicarbonate

ABSTRACT

Malignant tumours are characterised by a low, acidic extracellular pH (pHe) which facilitates invasion and metastasis. Previous research has proposed the potential benefits of manipulating systemic pHe, and recent experiments have highlighted the potential for buffer therapy to raise tumour pHe, prevent metastases, and prolong survival in laboratory mice. To examine the physiological regulation of tumour buffering and investigate how perturbations of the buffering system (via metabolic/respiratory disorders or changes in parameters) can alter tumour and blood pHe, we develop a simple compartmentalised ordinary differential equation model of pHe regulation by the HCO_3^-/CO_2 buffering system. An approximate analytical solution is constructed and used to carry out a sensitivity analysis, where we identify key parameters that regulate tumour pHe in both humans and mice. From this analysis, we suggest promising alternative and combination therapies, and identify specific patient groups which may show an enhanced response to buffer therapy. In addition, numerical simulations are performed, validating the model against well-known metabolic/respiratory disorders and predicting how these disorders could change tumour pHe.

1. Introduction

Malignant tumours consume significantly higher amounts of glucose than corresponding normal tissues or benign tumours [1,2]. This increased glucose uptake is observed even in the presence of adequate levels of oxygen, a phenomenon referred to as aerobic glycolysis. The use of aerobic glycolysis by cancer cells was characterised as early as the 1930s and named the Warburg effect [3,4]. The inefficiency of this type of metabolism significantly contributes to the observed increased glucose uptake and a subsequently increased acid load.

Upregulated aerobic glycolysis is a hallmark of malignant cancers [1]. The high level of glycolysis results in increased production of H^+ ions, leading to an acidification of the tumour microenvironment. This has been well documented by experiments showing that solid tumour extracellular pH (pHe) is commonly 0.5–1 units lower than normal tissue (tumour pHe of 6.5–7 vs a normal tissue pHe of 7.4) [5–7].

Despite the early discovery of the Warburg effect, little is understood about the reasons why malignant tumours consistently upregulate the use of aerobic glycolysis. In a series of papers, Gatenby et al. hypothesised that tumour acidification confers an advantage to the tumour cells, by producing a harsh environment in the peritumoural soft tissues as acid is transported along concentration gradients from the tumour in adjacent normal regions. This results in normal cell death, extracellular matrix degradation, increased angiogenesis and disordered immune response facilitating tumour invasion [8,4,1,9,10,2]. This 'acid mediated invasion hypothesis' is supported by experiments which have shown that normal cells proliferate optimally at a pHe of 7.4, with a steep decrease in proliferative ability below 7.1, while tumour cells obtain an optimal proliferation rate at pHe 6.8, which correlates with the slightly acidic environment found in invasive tumours [9].

The 'acid-mediated invasion hypothesis' leads to the prediction that neutralising the acidic tumour pHe will inhibit invasion and, subsequently, spontaneous metastasis, which has been explored in a recent set of experiments [11]. To test this prediction, Robey

* Corresponding author at: Department of Social Medicine, University of Bristol, Canynge Hall, 39 Whatley Road Bristol, BS8 2PS, UK. Tel.: +44 (0)7817 286755; fax: +44 (0)1865 283882.
E-mail address: natasha.martin@bristol.ac.uk (N.K. Martin).

0025-5564/$ - see front matter © 2010 Elsevier Inc. All rights reserved.
doi:10.1016/j.mbs.2010.12.002

et al. implanted highly metastatic human breast cancer cells in the mammary fat pad of severe combined immunodeficient mice. Oral administration of sodium bicarbonate (which acts as a buffer to resist changes in pHe) raised primary tumour pHe, reduced the number and size of metastases, and prolonged survival [11]. More generally, Gatenby and Gawlinski [4] propose that manipulation of systemic pHe (either through acidification or alkalinisation) could reduce tumour growth by perturbing the system from the optimal pHe for tumour proliferation.

To examine how manipulation of the systemic buffering system can alter tumour pHe, we develop a simple but realistic model of tumour pHe regulation via the HCO_3^-/CO_2 system, including the effects of physiological control of blood buffering, detailed in Section 2. With this model, we explore model behaviour by constructing an asymptotic approximation (Section 2.2) and subsequently perform a sensitivity analysis to ascertain the key parameters regulating tumour pHe, and identify which of those parameters can be altered with minimal effect on blood pHe regulation (Section 3.4). Additionally, we model respiratory and metabolic disordered states, comparing blood pHe predictions to known data, and predicting the resulting effect on tumour pHe (Section 3.1).

2. Mathematical model

2.1. Model formulation and construction

To produce a basic model of blood and tumour buffering we first develop a simple model of the main extracellular buffering system, the HCO_3^-/CO_2 system, along with the physiological regulation of this system. The aim is to develop a simple model of pHe at the tumour and blood compartment scale which accurately models the physiological regulation of tumour and blood pHe. Although as a first approximation, we compare the behaviour of our model to known human data. Any additional buffering from intrinsic nonmotile buffers (such as proteins, amino acids, and phosphates) operate on a faster scale than the HCO_3^-/CO_2 buffer. As there is little to no movement of intrinsic buffers between compartments, we assume this contribution in the tumour tissue is constant and implicitly incorporated in the tumour proton production parameter. Furthermore, our model tracks arterial blood delivery to the tumour, which has haemoglobin in the oxygen-bound form with low proton carrying capacity. Consequently, it is reasonable to assume only a small proportion of blood delivered to hypoxic areas of the tumour will contain the deoxygenated form of haemoglobin which can bind protons. This hypoxic subcompartment would be low in bicarbonate, high in CO_2, and likely have poor flow and connectivity to the vascular network, and therefore would likely reduce the potential efficacy of any buffer delivery to that region. Subsequently, our model could be extended to include additional buffering components at different spatial and temporal scales. Hence, we consider a two-compartment model, simulating the blood and tumour tissue, incorporating the bicarbonate–carbon dioxide system. Crucially, the model also includes the physiological regulation of the bicarbonate system through ventilation and kidney filtration. In this respect, our model can be seen as an extension of the work of [12], and our analysis will show that inclusion of these effects can significantly affect model predictions. As we are interested in average tumour pHe and not pHe differences within the tumour, we neglect fine scale spatial variations in tumour acid production. Hence, we can subsequently ignore regional variation in oxygen levels and consumption as considered in previous models [12] and assume an average acid production rate. Furthermore, as tumour cells exhibiting the glycolytic phenotype rely on glycolysis even in the presence of oxygen, the local oxygen concentration should not significantly alter acid production.

The schematic for the mathematical model is shown in Fig. 1. We have that $B_{t,b}$ represents the concentration of bicarbonate per volume in the tumour and blood, respectively, in units of mol/L. $H_{t,b}$ represents the volumetric concentration of free protons within the tumour and blood, respectively, in units of mol/L. $C_{t,b}$ represents the concentration of carbon dioxide for the tumour and blood, respectively, in units of mol/L. Note that as we are modelling extracellular pH, we model the levels of ions in the tumour interstitial fluid surrounding the cells, and neglect the intracellular pH of the tumour cells themselves.

Each equation includes a term describing the chemical buffering reactions of the HCO_3^-/CO_2 system, which proceeds as follows:

$$HCO_3^- + H^+ \underset{k_2}{\overset{k_1}{\rightleftharpoons}} CO_2 + H_2O. \tag{1}$$

The first two terms in each equation describe this chemical buffering reaction, with k_2 and k_1 the reaction rate constants. This reaction is accelerated by the presence of the enzyme carbonic anhydrase (CA), the activity of which varies depending on the isozyme type. In our model, we include the action of carbonic anhydrase in both the blood and tumour by increasing the rate constants of the reaction to reflect this acceleration. The fastest acceleration occurs in the blood, where CA II in red blood cells can accelerate the hydration reaction 50 000 to 1 000 000 fold over the uncatalyzed rate at human body temperature [13]. Tumour associated carbonic anhydrases include CA II and CA IX [14], and the activity of CA IX has recently been found to be as high as CA II [15]. Hence, we assume for simplicity that the catalytic rates in the blood and tumour tissue are equal. Further, the asymptotic analysis indicates that the model is robust to changes of several orders of magnitude of these parameters (provided the pK_a, and hence ratio of the kinetic parameters, remains equal), as this will only alter the fast reaction timescale as the solution relaxes to the intermediate and slow solutions.

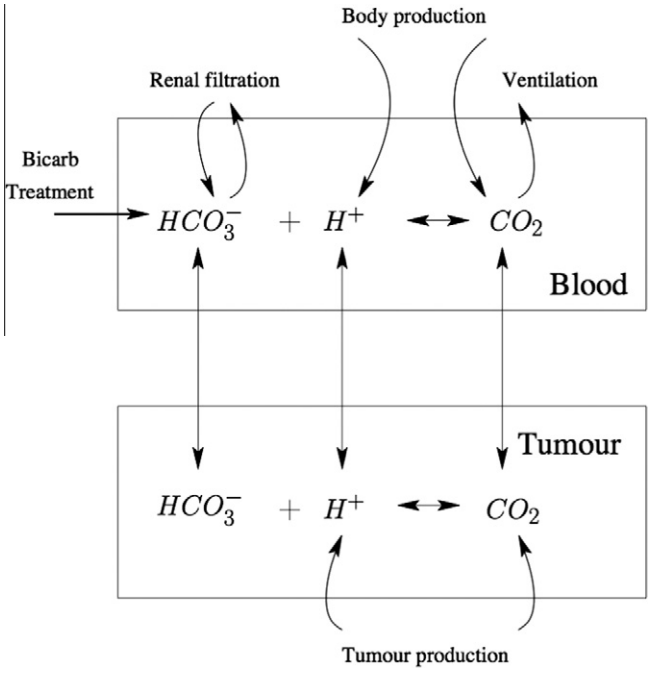

Fig. 1. Schematic of the systemic buffering model presented in Eqs. (2)–(7). The two compartments, blood and tumour, are linked through the vascular transfer of protons and buffering components such as carbon dioxide (CO_2) and bicarbonate (HCO_3^-). In the blood, various physiological systems such as ventilation and renal filtration tightly regulate the buffering system.

The equations also include a vascular exchange term for the respective ion or molecule between the blood and the tumour. Hence, γ_1, γ_2, γ_3 are the vessel flux rates for bicarbonate, lactate, and carbon dioxide, respectively. The vessel fluxes are calculated by $\gamma_i = VAD \times P_i$ where VAD is the vessel length per tumour cross section area (in cm/cm^2), and P_i is the vessel permeability (in cm/s) for the respective ion or molecule [16]. In order to ensure conservation of total quantities of H^+, CO_2 and HCO_3^- during the vascular exchange process from the tumour to the blood, we multiply γ_i by v_T, where $v_T = V_{tumour}/V_{blood}$, and where V_{tumour} is the volume of the tumour and V_{blood} is the volume of blood. Although tumour volume varies over time, the timescale of tumour growth is much slower than the pHe regulation dynamics examined in this model, and we therefore assume tumour size is constant. Furthermore, the sensitivity analysis in Section 3.4 indicates the system is not sensitive to this parameter.

The first three equations capture the tumour dynamics, and will be discussed in turn below.

$$\frac{dB_t}{dt} = \overbrace{k_2C_t - k_1B_tH_t}^{\text{chemical reactions}} + \overbrace{\gamma_1(B_b - B_t)}^{\text{vascular exchange}}. \tag{2}$$

Eq. (2) describes the bicarbonate dynamics in the tumour. As there is no direct production or consumption of HCO_3^- in the tumour, this equation only includes chemical reaction terms and vascular exchange of HCO_3^- between the blood and the tumour, where γ_1 is the vessel flux for bicarbonate.

$$\frac{dH_t}{dt} = \overbrace{k_2C_t - k_1B_tH_t}^{\text{chemical reactions}} + \overbrace{\phi_1}^{\text{tumour production}} - \overbrace{\gamma_2(H_t - H_b)}^{\text{vascular exchange}}. \tag{3}$$

Eq. (3) models the tumour H^+ concentration. The third term, ϕ_1, is the net production of H^+ per unit volume of the tumour through aerobic glycolysis, implicitly incorporating the fixed contribution of minor additional non-motile tissue buffering components which act on a faster timescale than the other reactions detailed. It is this production term that is generally higher than normal tissue due to the upregulation of glycolysis in malignant tumours. The final term is the vascular exchange, where γ_2 is the vessel flux for lactate as protons move in association with lactate to maintain electroneutrality.

$$\frac{dC_t}{dt} = \overbrace{k_1B_tH_t - k_2C_t}^{\text{chemical reactions}} + \overbrace{\phi_5}^{\text{tumour production}} - \overbrace{\gamma_3(C_t - C_b)}^{\text{vascular exchange}}. \tag{4}$$

Eq. (4) represents the tumour CO_2 dynamics. The third term, ϕ_5, represents the tumour production of CO_2 from cellular metabolism.

The last three equations capture the blood dynamics, and will be presented in turn. Firstly:

$$\frac{dB_b}{dt} = \overbrace{k_2C_b - k_1B_bH_b}^{\text{chemical reactions}} + \overbrace{\phi_2C_b - \lambda_1B_b}^{\text{kidney filtration}} + \overbrace{\theta_1}^{\text{treatment}} - \overbrace{\gamma_1 v_T(B_b - B_t)}^{\text{vascular exchange}}. \tag{5}$$

This equation describes the blood HCO_3^-. The third and fourth terms are standard representations used to model the complex process of renal filtration and reabsorption of bicarbonate [17,18]. The details of this system can be found in A. Briefly, an increase in blood CO_2 results in more conversion of CO_2 into HCO_3^- and H^+ inside the kidney nephrons, elevated levels of acid secretion into the bladder, and increased absorption of HCO_3^- into the bloodstream. If CO_2 levels are stable (through ventilation), then any increases in HCO_3^- result in an increased rate of renal bicarbonate filtration (and subsequent loss in the urine). Here, ϕ_2 is the acid secretion rate, and λ_1 is the bicarbonate filtration rate. The fifth term, θ_1, is the bicarbonate treatment term used in Robey et al. [11] study we examine in the sensitivity section.

$$\frac{dH_b}{dt} = \overbrace{k_2C_b - k_1B_bH_b}^{\text{chemical reactions}} + \overbrace{\phi_3}^{\text{body production}} + \overbrace{\gamma_2 v_T(H_t - H_b)}^{\text{vascular exchange}}. \tag{6}$$

Eq. (6) models the blood H^+ dynamics. The first two terms in Eq. (6) represent the bicarbonate buffering reaction kinetics in the blood. The third term represents the net contribution of protons from the rest of the body tissues (except for the tumour) after the contribution of non-motile tissue buffers.

$$\frac{dC_b}{dt} = \overbrace{k_1B_bH_b - k_2C_b}^{\text{chemical reactions}} + \overbrace{\phi_4}^{\text{body production}} - \overbrace{\lambda_2C_bf(C_b)}^{\text{ventilation}} + \overbrace{\gamma_3 v_T(C_t - C_b)}^{\text{vascular exchange}}. \tag{7}$$

Eq. (7) models the blood CO_2 concentration. The third term is the CO_2 source from the normal body tissues; here ϕ_4 represents the rate of CO_2 entry into the bloodstream from the normal tissue.

The fourth term in Eq. (7) represents the regulation of blood CO_2 levels by respiration, where CO_2 lost through ventilation is proportional to the product of the ventilation rate, $f(C_b)$, and the CO_2 concentration. The function for ventilation we use is:

$$f(C_b) = \begin{cases} V_{min} & \text{if } f(C_b) < V_{min}, \\ V_{slope}C_b - V_{intercept} & \text{if } V_{min} < f(C_b) < V_{max}, \\ V_{max} & \text{if } f(C_b) > V_{max}. \end{cases} \tag{8}$$

Note the linearity over a range with minimum and maximum thresholds [19]. Although the specific form of this term is a simplification of the complex dynamics surrounding ventilation, it is an appropriate approximation for the purposes of our model. The experimental ventilation response to blood CO_2 has been well quantified in both humans and mice and used to derive biological values for the ventilation parameters [20–22].

The initial conditions are $C_b(0) = c_0$, $C_t(0) = c_0$, $B_b(0) = b_0$, $B_t(0) = b_0$, $H_b(0) = h_0$, and $H_t(0) = h_0$. We choose c_0, b_0, and h_0 to be the standard blood values of CO_2, HCO_3^-, and H^+, respectively. This allows a clear visualisation of H^+ and CO_2 accumulation in the tumour, and subsequent depletion of HCO_3^-. Furthermore, as tumours can develop in many types of tissue with different metabolic rates, the baseline tissue values are likely to vary, but as there is only one steady-state the initial conditions do not affect the long-term behaviour of the system and are not a focus of this study.

In order to non-dimensionalise our model, we use the rescaling $\tau = k_2t$, $b_0b_t = B_t$, $c_0c_t = C_t$, $h_0h_t = H_t$, $b_0b_b = B_b$, $c_0c_b = C_b$, and $h_0h_b = H_b$ to obtain the system,

$$\frac{db_t}{d\tau} = \delta_1(c_t - \alpha_2b_th_t) + \Gamma_1(b_b - b_t), \tag{9}$$

$$\frac{dh_t}{d\tau} = \delta_3(c_t - \alpha_2b_th_t) + \Phi_1 - \Gamma_2(h_t - h_b), \tag{10}$$

$$\frac{dc_t}{d\tau} = -(c_t - \alpha_2b_th_t) + \Phi_5 - \Gamma_3(c_t - c_b), \tag{11}$$

$$\frac{db_b}{d\tau} = \delta_1(c_b - \alpha_2b_bh_b) + \Phi_2c_b - \xi_1b_b + \Theta_1 - \Gamma_1 v_T(b_b - b_t), \tag{12}$$

$$\frac{dh_b}{d\tau} = \delta_3(c_b - \alpha_2b_bh_b) + \Phi_3 + \Gamma_2 v_T(h_t - h_b), \tag{13}$$

$$\frac{dc_b}{d\tau} = -(c_b - \alpha_2b_bh_b) + \Phi_4 - \xi_3(c_b)c_b + \Gamma_3 v_T(c_t - c_b), \tag{14}$$

with $\delta_1 = \frac{c_0}{b_0}$, $\alpha_2 = \frac{k_1h_0b_0}{k_2c_0}$, $\Gamma_1 = \frac{\gamma_1}{k_2}$, $\delta_3 = \frac{c_0}{h_0}$, $\Phi_1 = \frac{\phi_1}{k_2h_0}$, $\Gamma_2 = \frac{\gamma_2}{k_2}$, $\Gamma_3 = \frac{\gamma_3}{k_2}$, $\Phi_2 = \frac{\phi_2c_0}{k_2b_0}$, $\xi_1 = \frac{\lambda_1}{k_2}$, $\Theta_1 = \frac{\theta_1}{k_2b_0}$, $\Phi_3 = \frac{\phi_3}{k_2h_0}$, $\Phi_4 = \frac{\phi_4}{k_2c_0}$, and $\Phi_5 = \frac{\phi_5}{k_2c_0}$.

Additionally, the non-dimensionalised ventilation function is now:

$$\xi_3(c_b) = \begin{cases} \Delta_{min} & \text{if } \xi_3(c_b) < \Delta_{min}, \\ \Delta_1c_b - \Delta_2 & \text{if } \Delta_{min} < \xi_3(c_b) < \Delta_{max}, \\ \Delta_{max} & \text{if } \xi_3(c_b) > \Delta_{max}, \end{cases} \tag{15}$$

with $\Delta_{min} = \frac{\lambda_2}{k_2}V_{min}$, $\Delta_1 = \frac{\lambda_2}{k_2}V_{slope}c_0$, $\Delta_2 = \frac{\lambda_2}{k_2}V_{intercept}$, and $\Delta_{max} = \frac{\lambda_2}{k_2}V_{max}$.

The initial conditions become:

$$c_b(0)=1,\ c_t(0)=1,\ b_b(0)=1,\ b_t(0)=1,\ h_b(0)=1,\ \text{ and }\ h_t(0)=1. \tag{16}$$

From the calculations detailed in A, the full parameter sets for a laboratory mouse and human are shown in Table 1. The non-dimensionalised values for a mouse and human are shown in Table 2.

2.2. Asymptotic simplification of the model

In this section we will construct a uniformly valid asymptotic approximation. This analytical solution is used to understand the general model behaviour and key parameter groupings. It is also used to perform a sensitivity analysis in Section 3.4 in order to examine which parameters have a large effect on tumour pHe. Potential treatments are then suggested which relate to the important parameters indicated by the sensitivity analysis.

Preliminary numerical simulations, as well as the wide variation in parameter values spanning several orders of magnitude, indicate different timescales in our solution. There are three characteristic timescales for our system. The inner, or fastest, is the timescale on which the reaction dynamics take place (k_1 and k_2 in Eqs. (2)–(7)). This is on the order of milliseconds. Then, there is an intermediate timescale where proton production takes place, on the order of seconds (ϕ_1 and ϕ_3 in Eqs. (3) and (6)). This intersects with a slower, outer solution which takes into account the rest of the physiology (kidney filtration, ventilation, etc.), and occurs on the scale of minutes to hours (ϕ_2, λ_1, λ_2 in Eqs. (5) and (7)). With this in mind, let us first examine the inner, fast solution.

2.2.1. Fast timescale dynamics

From our biological knowledge of the system, we know that the chemical reaction equations occur on the order of nano- to milliseconds, and are much faster than the other processes in our system. Furthermore, we can see that the parameter δ_3 is several orders of magnitude larger than any other, indicating that the $h_{t,b}$ equations will vary on the fast timescale (which is verified by proceeding with a standard asymptotic analysis). Thus we anticipate that chemical reactions will dominate the fast dynamics. To proceed, we define $\epsilon = 10^{-3}$, whereupon Eqs. (2)–(7) rescale to:

$$\frac{db_t}{d\tau}=\delta_1(c_t-\alpha_2 b_t h_t)+\epsilon^2\hat{\Gamma}_1(b_b-b_t), \tag{17}$$

$$\frac{dh_t}{d\tau}=\delta_3(c_t-\alpha_2 b_t h_t)+\epsilon\hat{\Phi}_1-\epsilon^2\hat{\Gamma}_2(h_t-h_b), \tag{18}$$

$$\frac{dc_t}{d\tau}=-(c_t-\alpha_2 b_t h_t)+\epsilon^2\hat{\Phi}_5-\epsilon^2\hat{\Gamma}_3(c_t-c_b), \tag{19}$$

$$\frac{db_b}{d\tau}=\delta_1(c_b-\alpha_2 b_b h_b)+\epsilon^2\hat{\Phi}_2 c_b-\epsilon^2\hat{\xi}_1 b_b+\epsilon^2\hat{\Theta}_1-\epsilon^2\hat{\Gamma}_1 v_T(b_b-b_t), \tag{20}$$

$$\frac{dh_b}{d\tau}=\delta_3(c_b-\alpha_2 b_b h_b)+\epsilon\hat{\Phi}_3+\epsilon^2\hat{\Gamma}_2 v_T(h_t-h_b), \tag{21}$$

$$\frac{dc_b}{d\tau}=-(c_b-\alpha_2 b_b h_b)+\epsilon^2\hat{\Phi}_4-\epsilon^2\hat{\xi}_3(c_b)c_b+\epsilon^2\hat{\Gamma}_3 v_T(c_t-c_b), \tag{22}$$

where $\delta_1=\frac{c_0}{b_0}$, $\alpha_2=\frac{k_1 h_0 b_0}{k_2 c_0}$, $\hat{\Gamma}_1=\frac{\gamma_1}{\epsilon^2 k_2}$, $\delta_3=\frac{c_0}{h_0}$, $\hat{\Phi}_1=\frac{\phi_1}{\epsilon k_2 h_0}$, $\hat{\Gamma}_2=\frac{\gamma_2}{\epsilon^2 k_2}$, $\hat{\Gamma}_3=\frac{\gamma_3}{\epsilon^2 k_2}$, $\hat{\Phi}_2=\frac{\phi_2 c_0}{\epsilon^2 k_2 b_0}$, $\hat{\xi}_1=\frac{\lambda_1}{\epsilon^2 k_2}$, $\hat{\Theta}_1=\frac{\theta_1}{\epsilon^2 k_2 b_0}$, $\hat{\Phi}_3=\frac{\phi_3}{\epsilon k_2 h_0}$, $\hat{\Phi}_4=\frac{\phi_4}{\epsilon^2 k_2 c_0}$, $\hat{\xi}_3(c_b)=\frac{\lambda_2}{\epsilon^2 k_2}f(c_b)$.

Table 2
Mouse and human non-dimensionalised parameter values.

Name	Mouse	Human
δ_1	5.0×10^{-2}	5.0×10^{-2}
Γ_1	2.5×10^{-8}	2.5×10^{-8}
δ_3	3.02×10^{4}	3.02×10^{4}
Φ_1	7.17×10^{-3}	7.17×10^{-3}
Γ_2	8.79×10^{-8}	8.79×10^{-8}
α_2	1.0	1.0
Φ_5	6.11×10^{-9}	7.63×10^{-9}
Γ_3	7.32×10^{-7}	7.32×10^{-7}
Φ_2	1.13×10^{-7}	2.11×10^{-8}
ξ_1	1.10×10^{-7}	1.90×10^{-8}
Θ_1	1.16×10^{-8}	9.16×10^{-10}
$v_T\Gamma_1$	2.5×10^{-9}	2.5×10^{-9}
Φ_3	1.28×10^{-3}	1.1×10^{-3}
$v_T\Gamma_2$	8.79×10^{-9}	8.79×10^{-9}
Φ_4	1.13×10^{-6}	9.16×10^{-8}
$v_T\Gamma_3$	7.32×10^{-8}	7.32×10^{-8}
Δ_{min}	5.23×10^{-7}	3.08×10^{-8}
Δ_1	1.52×10^{-6}	2.03×10^{-6}
Δ_2	3.51×10^{-7}	1.9×10^{-6}
Δ_{max}	2.05×10^{-6}	1.54×10^{-6}

Table 1
Mouse and human parameter values and sources. Details of the extraction and calculation of the parameters can be found in A. All citations of The Jackson Laboratory are in reference to the Mouse Tumor Biology Database (MTB), Mouse Genome Informatics, The Jackson Laboratory, Bar Harbor, Maine. The MTB is a database of laboratory mouse strain measurements of phenotypic and genotypic data [56]. The database is located at http://tumor.informatics.jax.org.

Name	Mouse	Human	Units	Source (M: mouse, H: Human)
h_0	3.98×10^{-8}	3.98×10^{-8}	mol/L	M: [35,36] H: [18]
b_0	2.4×10^{-2}	2.4×10^{-2}	mol/L	M: [35,36] H: [18]
c_0	1.2×10^{-3}	1.2×10^{-3}	mol/L	M: [35,36] H: [18]
P_1	3.4×10^{-5}	3.4×10^{-5}	cm/s	[16,37]
P_2	1.2×10^{-4}	1.2×10^{-4}	cm/s	[9]
P_3	1×10^{-3}	1×10^{-3}	cm/s	[38,39]
VAD	20	20	cm/cm^2	[40–42]
v_T	0.1	0.01	–	M: [11,43,57] H: [44,43]
ϕ_1	7.8×10^{-6}	7.8×10^{-6}	mol/L/s	fit to [11], within the range from [45,9]
ϕ_4	3.7×10^{-5}	3×10^{-6}	mol/L/s	M: [46,35,36] H: [46]
ϕ_2	6.16×10^{-2}	1.14×10^{-2}	1/s	M: [47] H: [17,18]
ϕ_3	1.5×10^{-6}	1.2×10^{-6}	mol/L/s	M: [45,35] H: [45,17]
ϕ_5	2×10^{-7}	2.5×10^{-7}	mol/L/s	M: [46,35] H: [46,17]
λ_1	3×10^{-3}	5.2×10^{-4}	1/s	M: [48,49,59] H: [18,50–52]
λ_2	102	0.042	1/L	M: [53] H: [17,18]
k_2	2.73×10^{4}	2.73×10^{4}	1/s	[13–15]
k_1	3.437×10^{10}	3.437×10^{10}	L/mol × s	from pK_a in [17,54]
V_{slope}	0.34	1.1×10^{3}	L^2/mol × s	M: [22,58] H: [20,21]
V_{max}	5.5×10^{-4}	1	L/s	M: [22] H: [20,21]
V_{min}	1.4×10^{-4}	0.02	L/s	M: [22] H: [20,21]
$V_{intercept}$	9.4×10^{-5}	1.237	L/s	M: [22] H: [20,21]
θ_1	7.6×10^{-6}	6×10^{-7}	mol/L × s	M: [11] H: [11,55]

The ventilation function becomes:

$$\hat{\xi}_3(c_b) = \begin{cases} \hat{\Delta}_{min} & \text{if } \xi_3(c_b) < \hat{\Delta}_{min}, \\ \hat{\Delta}_1 c_b - \hat{\Delta}_2 & \text{if } \hat{\Delta}_{min} < \hat{\xi}_3(c_b) < \hat{\Delta}_{max}, \\ \hat{\Delta}_{max} & \text{if } \hat{\xi}_3(c_b) > \hat{\Delta}_{max}, \end{cases} \tag{23}$$

with $\hat{\Delta}_{min} = \frac{\lambda_2}{\epsilon^2 k_2} V_{min}$, $\hat{\Delta}_1 = \frac{\lambda_2}{\epsilon^2 k_2} V_{slope} c_0$, $\hat{\Delta}_2 = \frac{\lambda_2}{\epsilon^2 k_2} V_{intercept}$, and $\hat{\Delta}_{max} = \frac{\lambda_2}{\epsilon^2 k_2} V_{max}$.

Note that we can decouple the reaction dynamics by making the following substitution: $u_1 = b_t + \delta_1 c_t$, $u_2 = b_b + \delta_1 c_b$, $v_1 = h_t + \delta_3 c_t$, $v_2 = h_b + \delta_3 c_b$. With these substitutions, Eqs. (17)–(22) become:

$$\frac{du_1}{d\tau} = \epsilon^2 \hat{\Gamma}_1 \left(u_2 - \frac{\delta_1}{\delta_3} v_2 + \frac{\delta_1}{\delta_3} h_b - u_1 + \frac{\delta_1}{\delta_3} v_1 - \frac{\delta_1}{\delta_3} h_t \right) + \delta_1 \epsilon^2 \hat{\Phi}_5 - \epsilon^2 \frac{\delta_1}{\delta_3} \hat{\Gamma}_3 (v_1 - h_t - v_2 + h_b), \tag{24}$$

$$\frac{dv_1}{d\tau} = \epsilon \hat{\Phi}_1 - \epsilon^2 \hat{\Gamma}_2 (h_t - h_b) + \delta_3 \epsilon^2 \hat{\Phi}_5 - \epsilon^2 \hat{\Gamma}_3 (v_1 - h_t - v_2 + h_b), \tag{25}$$

$$\frac{dh_t}{d\tau} = v_1 - h_t - \alpha_2 h_t (\delta_3 u_1 - \delta_1 v_1 + \delta_1 h_t) + \epsilon \hat{\Phi}_1 - \epsilon^2 \hat{\Gamma}_2 (h_t - h_b), \tag{26}$$

$$\begin{aligned} \frac{du_2}{d\tau} = {} & \epsilon^2 \hat{\Phi}_2 \left(\frac{1}{\delta_3} (v_2 - h_b) \right) - \epsilon^2 \hat{\xi}_1 \left(u_2 - \frac{\delta_1}{\delta_3} v_2 + \frac{\delta_1}{\delta_3} h_b \right) + \epsilon^2 \hat{\Theta}_1 \\ & - \epsilon^2 \hat{\Gamma}_1 v_T \left(u_2 - \frac{\delta_1}{\delta_3} v_2 + \frac{\delta_1}{\delta_3} h_b - u_1 + \frac{\delta_1}{\delta_3} v_1 - \frac{\delta_1}{\delta_3} h_t \right) \\ & + \delta_1 \epsilon^2 \hat{\Phi}_4 - \epsilon^2 \frac{\delta_1}{\delta_3} (v_2 - h_b) \hat{\xi}_3 \left(\frac{1}{\delta_3} (v_2 - h_b) \right) \\ & + \epsilon^2 \frac{\delta_1}{\delta_3} \hat{\Gamma}_3 v_T (v_1 - h_t - v_2 + h_b), \end{aligned} \tag{27}$$

$$\begin{aligned} \frac{dv_2}{d\tau} = {} & \epsilon \hat{\Phi}_3 + \epsilon^2 \hat{\Gamma}_2 v_T (h_t - h_b) + \delta_3 \epsilon^2 \hat{\Phi}_4 \\ & - \epsilon^2 (v_2 - h_b) \hat{\xi}_3 \left(\frac{1}{\delta_3} (v_2 - h_b) \right) \\ & + \epsilon^2 \hat{\Gamma}_3 v_T (v_1 - h_t - v_2 + h_b), \end{aligned} \tag{28}$$

$$\begin{aligned} \frac{dh_b}{d\tau} = {} & v_2 - h_b - \alpha_2 h_b (\delta_3 u_2 - \delta_1 v_2 + \delta_1 h_b) + \epsilon \hat{\Phi}_3 \\ & + \epsilon^2 \hat{\Gamma}_2 v_T (h_t - h_b). \end{aligned} \tag{29}$$

Our new variables $v_{1,2}$ are not scaled to order 1, in fact, they are $O(\delta_3) = O(10^4)$. However, the advantage is that the leading order equations then simplify on noting the size of $v_{1,2}$, yielding at leading order:

$$\frac{du_1}{d\tau} = \frac{dv_1}{d\tau} = 0, \tag{30}$$

$$\frac{dh_t}{d\tau} = v_1 - h_t - \alpha_2 h_t (\delta_3 u_1 - \delta_1 v_1 + \delta_1 h_t), \tag{31}$$

$$\frac{du_2}{d\tau} = \frac{dv_2}{d\tau} = 0, \tag{32}$$

$$\frac{dh_b}{d\tau} = v_2 - h_b - \alpha_2 h_b (\delta_3 u_2 - \delta_1 v_2 + \delta_1 h_b). \tag{33}$$

From these equations, we can see that u_1, v_1, u_2 and v_2 are constant, respectively denoted A_1, A_2, A_3, and A_4, and hence,

$$\frac{dh_t}{d\tau} = -\alpha_2 \delta_1 h_t^2 + (-1 - \delta_3 \alpha_2 A_1 + \delta_1 \alpha_2 A_2) h_t + A_2, \tag{34}$$

$$\frac{dh_b}{d\tau} = -\alpha_2 \delta_1 h_b^2 + (-1 - \delta_3 \alpha_2 A_3 + \delta_1 \alpha_2 A_4) h_b + A_4. \tag{35}$$

These equations have one positive, stable steady state given by

$$\tilde{h}_{t+} = \frac{(-1 - \delta_3 \alpha_2 A_1 + \delta_1 \alpha_2 A_2) + \sqrt{(-1 - \delta_3 \alpha_2 A_1 + \delta_1 \alpha_2 A_2)^2 + 4\alpha_2 \delta_1 A_2}}{2\alpha_2 \delta_1}, \tag{36}$$

$$\tilde{h}_{b+} = \frac{(-1 - \delta_3 \alpha_2 A_3 + \delta_1 \alpha_2 A_4) + \sqrt{(-1 - \delta_3 \alpha_2 A_3 + \delta_1 \alpha_2 A_4)^2 + 4\alpha_2 \delta_1 A_4}}{2\alpha_2 \delta_1}. \tag{37}$$

Therefore, in our original variables, the solution, which we will denote as W_{fast}, follows these equations:

$$\frac{dh_t}{d\tau} = -\alpha_2 \delta_1 h_t^2 + (-1 - \delta_3 \alpha_2 A_1 + \delta_1 \alpha_2 A_2) h_t + A_2, \tag{38}$$

$$\frac{dh_b}{d\tau} = -\alpha_2 \delta_1 h_b^2 + (-1 - \delta_3 \alpha_2 A_3 + \delta_1 \alpha_2 A_4) h_b + A_4, \tag{39}$$

$$c_t = \frac{1}{\delta_3} (A_2 - h_t), \tag{40}$$

$$c_b = \frac{1}{\delta_3} (A_4 - h_b), \tag{41}$$

$$b_t = A_1 - \frac{\delta_1}{\delta_3} A_2 + \frac{\delta_1}{\delta_3} h_t, \tag{42}$$

$$b_b = A_3 - \frac{\delta_1}{\delta_3} A_4 + \frac{\delta_1}{\delta_3} h_b. \tag{43}$$

In general, the model dynamics of interest on the intermediate and slow timescales are insensitive to the timescales of the fast reactions (providing the fast reactions remain fast). Hence, altering the specific kinetic parameters (but keeping the pK_a, and hence the ratio of these parameters, equal) does not alter the system behaviour on the timescales of interest.

2.2.2. Intermediate timescale dynamics

To examine the intermediate timescale dynamics, let us rescale time, so $\tau_2 = \epsilon\tau$. We have, at leading order, again noting that our variables $v_{1,2}$ are not scaled to order 1, but instead $O(\delta_3) = O(10^4)$,

$$\frac{du_1}{d\tau_2} = 0, \tag{44}$$

$$\frac{dv_1}{d\tau_2} = \hat{\Phi}_1 + \delta_3 \epsilon \hat{\Phi}_5 - \epsilon \hat{\Gamma}_3 (v_1 - v_2), \tag{45}$$

$$0 = -\alpha_2 \delta_1 h_t^2 + (-1 - \delta_3 \alpha_2 u_1 + \delta_1 \alpha_2 v_1) h_t + v_1, \tag{46}$$

$$\frac{du_2}{d\tau_2} = 0, \tag{47}$$

$$\frac{dv_2}{d\tau_2} = \hat{\Phi}_3 + \delta_3 \epsilon \hat{\Phi}_4 - \epsilon \left(\frac{\hat{\Delta}_1}{\delta_3} v_2^2 - \hat{\Delta}_2 v_2 \right) + \epsilon \hat{\Gamma}_3 v_T (v_1 - v_2), \tag{48}$$

$$0 = -\alpha_2 \delta_1 h_b^2 + (-1 - \delta_3 \alpha_2 u_2 + \delta_1 \alpha_2 v_2) h_b + v_2. \tag{49}$$

Thus we can see immediately that u_1 and u_2 are constant as previously and, respectively, denoted by A_1 and A_3. Further, h_t and h_b are at their slow dynamics steady states, given by Eqs. (36) and (37).

Hence, we are left with only two ODEs, Eqs. (45) and (48), where the initial conditions for v_1 and v_2 are the equilibrium values from the fast solution, A_2 and A_4, respectively.

Here we can see that the positive equilibrium solutions are:

$$\tilde{v}_2 = \frac{\epsilon \delta_3 \hat{\Delta}_2 + \delta_3 \sqrt{\epsilon^2 \hat{\Delta}_2^2 + 4\epsilon \frac{\hat{\Delta}_1}{\delta_3} (\hat{\Phi}_3 + \delta_3 \epsilon \hat{\Phi}_4 + v_T \hat{\Phi}_1 + \delta_3 \epsilon \hat{\Phi}_5 v_T)}}{2\epsilon \hat{\Delta}_1}, \tag{50}$$

$$\tilde{v}_1 = \frac{\epsilon \delta_3 \hat{\Delta}_2 + \delta_3 \sqrt{\epsilon^2 \hat{\Delta}_2^2 + 4\epsilon \frac{\hat{\Delta}_1}{\delta_3} (\hat{\Phi}_3 + \delta_3 \epsilon \hat{\Phi}_4 + v_T \hat{\Phi}_1 + \delta_3 \epsilon \hat{\Phi}_5 v_T)}}{2\epsilon \hat{\Delta}_1} + \frac{1}{\epsilon \hat{\Gamma}_3} \left(\hat{\Phi}_1 + \delta_3 \epsilon \hat{\Phi}_5 \right), \tag{51}$$

where standard linear analysis shows this steady state is stable.

Changing back into our original variables so we can compare our approximate analytical solution to our numerical simulations, the solutions (which we will denote as $W_{intermediate}$) satisfy these equations:

$$h_{t+} = \frac{(-1-\delta_3\alpha_2 A_1 + \delta_1\alpha_2 v_1) + \sqrt{(-1-\delta_3\alpha_2 A_1 + \delta_1\alpha_2 v_1)^2 + 4\alpha_2\delta_1 v_1}}{2\alpha_2\delta_1}, \tag{52}$$

$$h_{b+} = \frac{(-1-\delta_3\alpha_2 A_3 + \delta_1\alpha_2 v_2) + \sqrt{(-1-\delta_3\alpha_2 A_3 + \delta_1\alpha_2 v_2)^2 + 4\alpha_2\delta_1 v_2}}{2\alpha_2\delta_1}, \tag{53}$$

$$c_t = \frac{1}{\delta_3}(v_1 - h_t), \quad c_b = \frac{1}{\delta_3}(v_2 - h_b), \tag{54}$$

$$b_t = A_1 - \frac{\delta_1}{\delta_3}(v_1 - h_t), \quad b_b = A_3 - \frac{\delta_1}{\delta_3}(v_2 - h_b), \tag{55}$$

where v_1 and v_2 are determined by the solution to Eqs. (45) and (48).

2.2.3. Slow timescale dynamics

The final, slow timescale, is where the physiological responses such as ventilation and kidney excretion take effect. To examine the slow dynamics, let us rescale time, defining $\tau_3 = \epsilon^2\tau$. Once again we note that $v_{1,2}$ are $O(\delta_3) = O(10^4)$, hence we consider each term in turn when approximating to leading order. Thus we have at leading order,

$$\frac{du_1}{d\tau_3} = \hat{\Gamma}_1\left(u_2 - \frac{\delta_1}{\delta_3}v_2 - u_1 + \frac{\delta_1}{\delta_3}v_1\right) + \delta_1\hat{\Phi}_5 - \hat{\Gamma}_3\frac{\delta_1}{\delta_3}(v_1 - v_2), \tag{56}$$

$$0 = \hat{\Phi}_1 + \delta_3\epsilon\hat{\Phi}_5 - \epsilon\hat{\Gamma}_3(v_1 - v_2), \tag{57}$$

$$0 = -\alpha_2\delta_1 h_t^2 + (-1 - \delta_3\alpha_2 u_1 + \delta_1\alpha_2 v_1)h_t + v_1, \tag{58}$$

$$\begin{aligned}\frac{du_2}{d\tau_3} = {} & \frac{\hat{\Phi}_2}{\delta_3}v_2 - \hat{\xi}_1\left(u_2 - \frac{\delta_1}{\delta_3}v_2\right) + \hat{\Theta}_1 \\ & - \hat{\Gamma}_1 v_T\left(u_2 - \frac{\delta_1}{\delta_3}v_2 - u_1 + \frac{\delta_1}{\delta_3}v_1\right) + \delta_1\hat{\Phi}_4 - \frac{\delta_1\hat{\Delta}_1}{\delta_3^2}v_2^2 \\ & + \frac{\delta_1\hat{\Delta}_2}{\delta_3}v_2 + \hat{\Gamma}_3 v_T\frac{\delta_1}{\delta_3}(v_1 - v_2),\end{aligned} \tag{59}$$

$$0 = \hat{\Phi}_3 + \delta_3\epsilon\hat{\Phi}_4 - \epsilon\left(\frac{\hat{\Delta}_1}{\delta_3}v_2^2 - \hat{\Delta}_2 v_2\right) + \epsilon\hat{\Gamma}_3 v_T(v_1 - v_2), \tag{60}$$

$$0 = -\alpha_2\delta_1 h_b^2 + (-1 - \delta_3\alpha_2 u_2 + \delta_1\alpha_2 v_2)h_b + v_2. \tag{61}$$

The initial conditions are the intermediate timescale equilibrium values for $u_{1,2}$ (denoted A_1 and A_3). As these equations are linear in u_1 and u_2, they can be solved explicitly. The equilibrium values, which are both positive with our parameters, are

$$\tilde{u_2} = \frac{1}{\hat{\xi}_1}\left(\frac{\hat{\Phi}_2}{\delta_3}v_2 + \frac{\hat{\xi}_1\delta_1}{\delta_3}v_2 + \hat{\Theta}_1 + \delta_1 v_T\hat{\Phi}_5 + \delta_1\hat{\Phi}_4 - \frac{\delta_1\hat{\Delta}_1}{\delta_3^2}v_2^2 + \frac{\delta_1\hat{\Delta}_2}{\delta_3}v_2\right), \tag{62}$$

$$\tilde{u_1} = \tilde{u_2} - \frac{\delta_1}{\delta_3}v_2 + \frac{\delta_1}{\delta_3}v_1 + \frac{1}{\hat{\Gamma}_1}\left(\delta_1\hat{\Phi}_4 - \frac{\delta_1\hat{\Gamma}_3}{\delta_3}[v_1 - v_2]\right). \tag{63}$$

Standard linear analysis shows that this equilibrium point is a linearly stable node.

Changing back into our original variables in order to calculate and compare our approximate analytical solution to our numerical solution, the slow solutions (which we will denote as W_{slow}), follow these equations,

$$h_t = \frac{(-1-\delta_3\alpha_2 u_1 + \delta_1\alpha_2 v_1) + \sqrt{(-1-\delta_3\alpha_2 u_1 + \delta_1\alpha_2 v_1)^2 + 4\alpha_2\delta_1 v_1}}{2\alpha_2\delta_1}, \tag{64}$$

$$h_b = \frac{(-1-\delta_3\alpha_2 u_2 + \delta_1\alpha_2 v_2) + \sqrt{(-1-\delta_3\alpha_2 u_2 + \delta_1\alpha_2 v_2)^2 + 4\alpha_2\delta_1 v_2}}{2\alpha_2\delta_1}, \tag{65}$$

$$c_t = \frac{1}{\delta_3}(v_1 - h_t), \tag{66}$$

$$c_b = \frac{1}{\delta_3}(v_2 - h_b), \tag{67}$$

$$b_t = u_1 - \frac{\delta_1}{\delta_3}(v_1 - h_t), \tag{68}$$

$$b_b = u_2 - \frac{\delta_1}{\delta_3}(v_2 - h_b), \tag{69}$$

where $v_{1,2}$ and $h_{t,b}$ are defined by the algebraic Eqs. (57), (58), (60) and (61) and $u_{1,2}$ are the solutions to the ODEs in Eqs. (56) and (59). The explicit large time asymptote, steady state, solutions can be readily found, yielding the steady state solutions in our original variables:

$$\tilde{h}_t = \frac{(-1-\delta_3\alpha_2\tilde{u}_1 + \delta_1\alpha_2 v_1) + \sqrt{(-1-\delta_3\alpha_2\tilde{u}_1 + \delta_1\alpha_2 v_1)^2 + 4\alpha_2\delta_1 v_1}}{2\alpha_2\delta_1}, \tag{70}$$

$$\tilde{h}_b = \frac{(-1-\delta_3\alpha_2\tilde{u}_2 + \delta_1\alpha_2 v_2) + \sqrt{(-1-\delta_3\alpha_2\tilde{u}_2 + \delta_1\alpha_2 v_2)^2 + 4\alpha_2\delta_1 v_2}}{2\alpha_2\delta_1}, \tag{71}$$

$$\tilde{c}_t = \frac{1}{\delta_3}(v_1 - \tilde{h}_t), \tag{72}$$

$$\tilde{c}_b = \frac{1}{\delta_3}(v_2 - \tilde{h}_b), \tag{73}$$

$$\tilde{b}_t = \tilde{u}_1 - \frac{\delta_1}{\delta_3}(v_1 - \tilde{h}_t), \tag{74}$$

$$\tilde{b}_b = \tilde{u}_2 - \frac{\delta_1}{\delta_3}(v_2 - \tilde{h}_b), \tag{75}$$

where v_1 and v_2 are the steady state solutions from the intermediate timescale in Eq. (50) and (51), respectively. Also, $\tilde{u}_1$ and $\tilde{u}_2$ are the steady state solutions of Eqs. (56) and (59).

By extracting the leading order terms with our chosen parameters, we find,

$$\tilde{h}_t = \frac{\left(\frac{\delta_3\hat{\Delta}_2}{\hat{\Delta}_1} + \frac{\hat{\Phi}_1}{\epsilon\hat{\Gamma}_3}\right)}{\delta_3\alpha_2\left(\frac{\hat{\Phi}_2\hat{\Delta}_2}{\hat{\xi}_1\hat{\Delta}_1} - \frac{\delta_1\hat{\Phi}_1}{\hat{\Gamma}_1\delta_3\epsilon}\right)} + O\left(\frac{1}{\delta_3}\right). \tag{76}$$

From Eq. (76) we can see that to leading order, $\tilde{h}_t$ is proportional to $\hat{\xi}_1$ and inversely proportional to α_2, $\hat{\Gamma}_3$, $\hat{\Gamma}_1$, and $\hat{\Phi}_2$. Therefore, lowering the glomerular filtration rate (ξ_1) will lower H^+ levels in the tumour. Conversely, raising the acid secretion rate (Φ_2), carbon dioxide vessel permeability (Γ_3), or bicarbonate vessel permeability (Γ_1) will lower tumour H^+. This expression can tell us about how groups of parameters affect the long time steady-state, and allows us to identify the most important ones. However, quantification of

the relative importance with this expression is difficult, so we will proceed with a formal sensitivity analysis in Section 3.4 after we construct the uniformly valid solution.

2.2.4. Uniformly valid solution

It is now straightforward to construct an approximate uniformly valid solution using our fast, intermediate, and slow solutions from above. This uniform solution has the form:

$$W_{uniform} = W_{fast} + W_{intermediate} + W_{slow} - \tilde{W}_{fast} - \tilde{W}_{intermediate}, \qquad (77)$$

where $\tilde{W}_{fast,intermediate}$ are the quasi-steady state solutions to the W_{fast} and $W_{intermediate}$ equations, respectively.

2.2.5. Sensitivity analysis

It is important to identify how sensitive the system is to the chosen parameter values. Most importantly, we would like to be able to predict treatments targeting the parameters that have the most pronounced effect on raising tumour pHe. In particular, we are most interested in the parameters which have the greatest effect in lowering the steady state tumour pHe, as well as how the treatment term can affect the pHe of the tumour and the blood. Also, as parameter variations exist naturally between patients, if the system is particularly sensitive to a given parameter it would be important to highlight this system behaviour. As noted, the previously derived analytical approximation can tell us about how groups of parameters affect the long time steady-state, but it is difficult to quantify the relative importance of each individual parameter contribution. Hence, analytical sensitivity values can provide this added information.

One way of examining the effect of a parameter, p, on one of our steady state variables, V, is to calculate a sensitivity coefficient. This can be defined as

$$S_{V,p} = \frac{p}{V}\frac{\partial V}{\partial p}. \qquad (78)$$

The calculation of this sensitivity coefficient, S, tells us what effect a percentage change in the parameter, p, has on the variable, V. If $|S| > 1$, a percent change in p produces a larger percent change in V, and thus p has a strong effect on V.

The analytical value of the sensitivity coefficient was calculated in Maple, and the parameter values were then substituted to obtain the numerical value.

2.2.6. Description of numerical methods

The model Eqs. (9)–(14) were solved using the Matlab stiff ODE solver ode15s, a variable order multistep solver. A stiff solver is necessary due to the multiple timescales in this system, with rapid transient movement of the reaction kinetics, and then slowly varying long transients. Initial conditions were used as in (16) and parameters from Table 1. The simulations were run until $\tau = 1 \times 10^{10}$ to ensure steady state is reached.

3. Results

3.1. Model validation: comparison of respiratory/metabolic disorders to observed blood pHe

In this section we present a set of numerical simulations of Eqs. (9)–(14) to confirm that the model produces qualitatively and quantitatively reasonable and accurate results.

In order to confirm that the mathematical model correctly simulates blood pHe, we examine the accuracy of the model in a variety of clinical situations which we can compare to data. In the unperturbed system, the blood pHe equilibrates at the normal blood value of 7.4 (see Fig. 2), with blood carbon dioxide and bicarbonate concentrations also at their normal values (non-dimensionalised to 1).

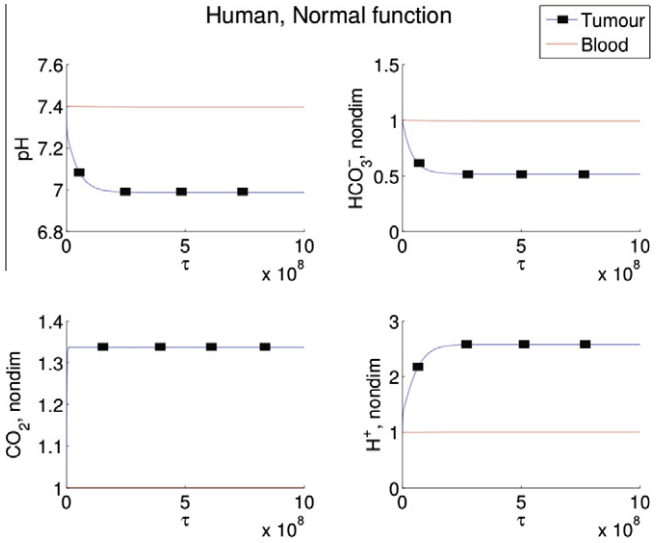

Fig. 2. Simulations of Eqs. (9)–(14) for human blood (solid line) and tumour (line with squares) values of pHe (top left), HCO_3^- (top right), CO_2 (bottom left), and H^+ (bottom right) levels, with no metabolic or respiratory disorder, and no bicarbonate treatment. Note the blood pHe remains at 7.4, with normal levels of HCO_3^- and CO_2. By contrast, the tumour has a lowered pHe to 7.0, with elevated CO_2 and low HCO_3^- levels. The numerical simulations are run with initial conditions (16) and parameters as in Table 1 but with $\theta_1 = 0$. Note that τ of 10^9 corresponds to a dimensional time of approximately 10 h.

Four disordered states are then simulated: respiratory alkalosis, metabolic alkalosis, respiratory acidosis, and metabolic alkalosis. In our simulations, the respiratory disorders are induced by fixing the ventilation rate, $\xi_3(c_b)$, at higher or lower values than normal, thereby changing the blood CO_2 levels. Metabolic disorders are induced by altering the blood HCO_3^- levels by the addition or removal of bicarbonate (θ_1). These results are shown in Figs. 3 and 4. For the respiratory disturbance scenarios, in agreement with experiments which induce patients to hyperventilate or hypoventilate, the ventilation rate is fixed and varied to produce either acidosis or alkalosis. Initially, change in ventilation rate causes a change in blood CO_2, which immediately alters the HCO_3^- and H^+ levels. After a few hours the effects of the renal compensation are visible, with the amount of reabsorbed bicarbonate changing to compensate and push the pHe back to normal. Both of these simulated disorders match the correct clinically predicted pHe and compensation timescale [17]. Simulations of metabolic disorders (acidosis or alkalosis) as a result of persistent administration of bicarbonate (due to bicarbonate loading) or loss of bicarbonate (for example, through vomiting) predict no respiratory compensation, hence blood pHe levels do not return to normal.

To compare our results more rigorously with clinical data on acid/base disturbances, a standard buffer curve of the blood pHe is constructed. This is accomplished by inducing a respiratory or metabolic disturbance into the model (as described above), and tracking blood pHe prior to renal compensation. Although in these simulations we are primarily interested in the blood dynamics, the full coupled model is simulated (blood and tumour). This is reasonable as the tumour of our simulated size has a negligible effect on blood dynamics (results not shown, but the model sensitivity is calculated in Section 3.4).

The simulated results and clinical buffer curves for humans are shown in Fig. 5. The mathematical model performs well, particularly in predicting the response to metabolic disorders, and also in our range of interest (a normal blood of pHe 7.35–7.45). For

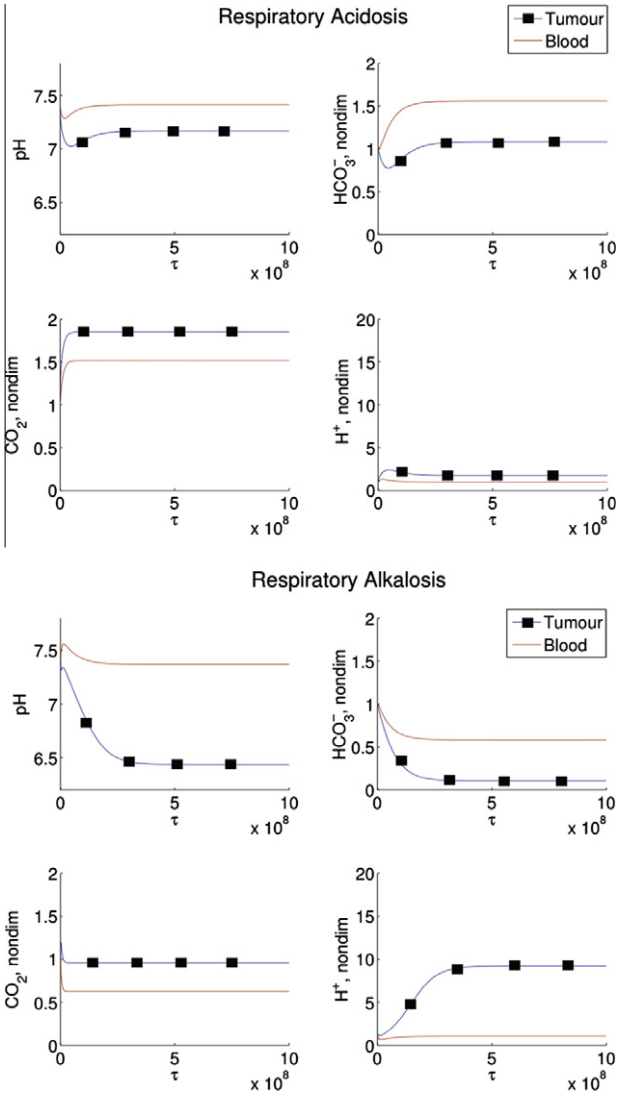

Fig. 3. Simulated respiratory disorders in humans. Induced respiratory acidosis (top panels) and induced respiratory alkalosis (bottom panels). In both situations, there is an initial blood pHe alteration due to the respiratory disturbance. However, after a few hours, the effect of renal compensation is visible, pushing the pHe back to normal and resulting in altered bicarbonate and carbon dioxide levels. In this simulation, Eqs. (9)–(14) are solved with initial conditions (16) and parameters as in Table 1 except the change in $\xi_3(c_b)$ ($\xi_3(c_b) = 7.7 \times 10^{-8}$ for respiratory acidosis, $\xi_3(c_b) = 2.3 \times 10^{-7}$ for respiratory alkalosis), and with $\theta_1 = 0$. Note that τ of 10^9 corresponds to a dimensional time of ≈10 h.

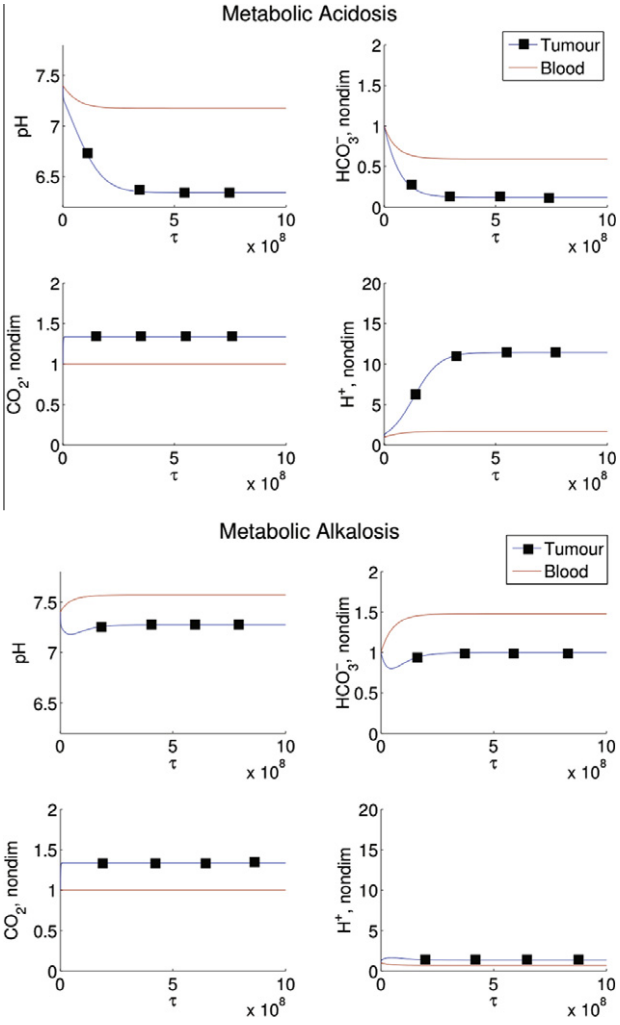

Fig. 4. Simulated metabolic disorders in humans. Results are shown for induced metabolic acidosis (top panels) and induced metabolic alkalosis (bottom panels). Elevations (reductions) in blood pHe result in subsequent increases (decreases) in tumour pHe. Additionally, acidification of the bloodstream can cause substantial reductions in tumour pHe, potentially to toxic levels for tumour cells. In this simulation, Eqs. (9)–(14) are solved with initial conditions (16) and parameters as in Table 1 except with $\theta_1 = -5 \times 10^{-6}$ in metabolic acidosis and $\theta_1 = 4 \times 10^{-6}$ in metabolic alkalosis.

example, the pHe changes caused by altering the amount of bicarbonate in the blood (for example, by changing θ_1 as is done in the simulations, or by impaired renal function which could affect Φ_2 or ξ_1) are shown by the squares in Fig. 5. The resulting curve follows a contour line of constant pCO_2 at 40 mm Hg, the normal level, as tight regulation of ventilation prevents any change in CO_2 levels. As this model is primarily interested in the effect of adding bicarbonate in this way, the accuracy of the simulations is encouraging.

Alternatively, the pHe changes caused by altering the CO_2 levels by fixing the ventilation rate, $\xi_3(c_b)$ (clinically induced via rebreathing CO_2 or hyperventilating), follow the triangles in Fig. 5. As shown in the previous section, respiratory disturbances immediately alter blood pHe and bicarbonate levels. Eventually, renal compensation occurs (both clinically and in our simulation), which is not shown in this figure as the *in vivo* studies were performed on a short timescale before compensation could occur. Again, the model performs well, despite the approximations to the CO_2/ventilation term, falling well within the 95% confidence limits of the data within the biological pHe range we are examining (7.35–7.45). Only at very low pHe is there a deviation from the predicted buffer line, which is acceptable particularly as the model is developed specifically to examine metabolic alkalosis (possibly induced by the bicarbonate treatment), not acidosis.

3.2. Model prediction: effect of respiratory/metabolic disorders on tumour pHe

Simulations of respiratory and metabolic disorders indicate that these disordered states can cause significant changes in tumor pHe. The model predicts tumor pHe is elevated (greater than 7.1 from a normal tumor pHe of 7.0) during the conditions of respiratory acidosis and metabolic alkalosis. During states of respiratory alkalosis and metabolic acidosis, tumor pHe can be lowered to potentially toxic levels for tumour cells (less than 6.5 from a normal tumor pHe of 7.0).

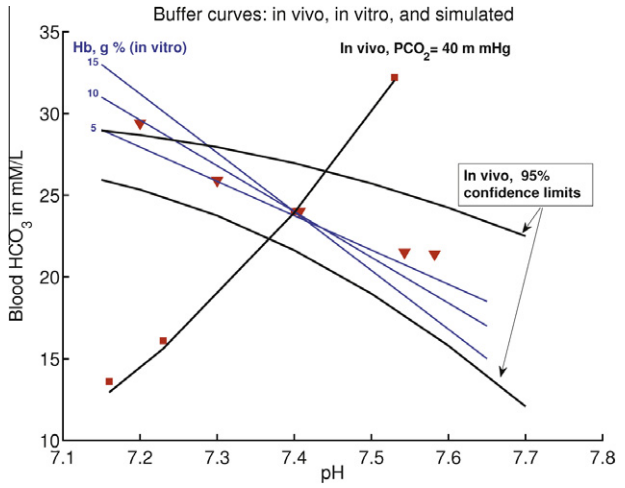

Fig. 5. Human buffer curve comparison between *in vitro*, *in vivo*, and calculated with our model. Blue lines represent *in vitro* curves of blood containing varying amounts of haemoglobin. Dark black lines are the *in vivo* observed ranges in values for a normal human. Red squares and triangles represent calculated values when Eqs. (9)–(14) are solved with initial conditions (16) and parameters as in Table 1 but with varying ζ_3 to simulate impaired ventilation, and varying θ_1 to simulate ingestion or loss of bicarbonate. Red squares represent inducing a metabolic disturbance by varying HCO_3^- (θ_1) with a constant pCO_2 level (40 mm Hg). The accuracy of the mathematical model, particularly with regards to metabolic alkalosis, is encouraging. Red triangles represent the effect of varying CO_2 through disordered ventilation. These data points were obtained by fixing ventilation rate, ζ_3, at several values, running the simulations as in Fig. 3, and taking the blood CO_2, HCO_3^-, and pHe values prior to renal compensation consistent with experiments. Although this model does not focus on respiratory disturbances, it still provides a good fit to data in this region, particularly in the region of interest where blood pHe is in the normal and safe region of 7.35–7.45. *In vitro* and *in vivo* data adapted with permission from The University of Chicago Press (Figures 17 and 18 in [18]). (For interpretation of the references to colours in this figure legend, the reader is referred to the web version of this paper.)

3.3. Comparison of numerical solutions and asymptotic approximations

Fig. 6 shows the uniform solution, Eq. (77), plotted against the numerical simulation, and agreement is excellent. The numerical solution is simulated with Eqs. (9)–(14). For the purposes of this comparison, the numerical and analytical solutions are calculated with initial conditions (16) and parameters from Table 2 but with $\Theta_1 = 0$.

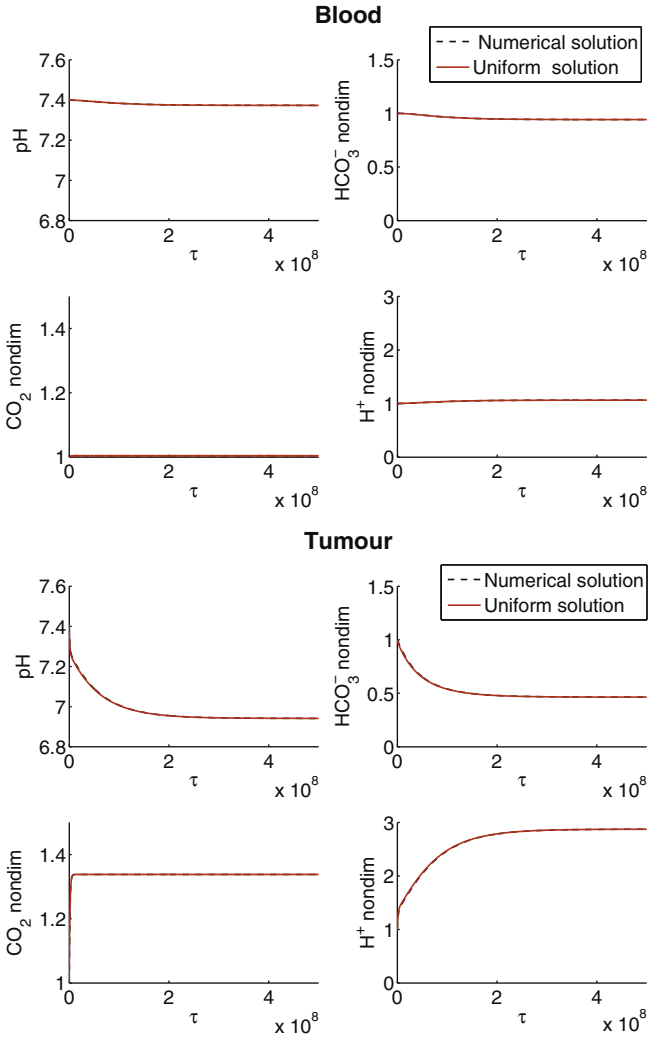

Fig. 6. Comparison of the numerical (black dashed line) and uniform analytical approximation (red line) in the (a) blood and (b) tumour in an untreated human. The uniform analytical solution is calculated from Eq. (77). The numerical solution is simulated with Eqs. (9)–(14). All numerical and analytical solutions are calculated with initial conditions (16) and parameters from Table 1 but with $\theta_1 = 0$. (For interpretation of the references to colours in this figure legend, the reader is referred to the web version of this paper.)

3.4. Modelling therapy: sensitivity analysis

The full results of the sensitivity analysis are presented in, Appendix Table 3.B, which displays the sensitivity of all the variables to each of the parameters for both mice and humans in the untreated and treated cases. The results are similar for both cases. The human and mouse tumour H^+ sensitivity coefficients with the largest effect on tumour pHe (selected by an absolute value greater than 1) are shown in Fig. 7. In both humans and mice, the sensitivity coefficients indicate that the most important parameters affecting the tumour pHe are those involved with renal function: bicarbonate clearance and reabsorption. Targeting these processes not only raises the tumour pHe, but also increases the bicarbonate therapy efficacy (simulations not shown).

Other key parameters which most significantly affect tumour pHe are $\hat{\Phi}_1$, which incorporates the tumour proton production rate, and the pK_a parameter $\hat{\alpha}_2$. In humans, the ventilation parameters ($\hat{\Delta}_1$ and $\hat{\Delta}_2$) are predicted to be very important, but less so in the mouse. Treatments which target renal parameters ($\hat{\xi}_1$ and $\hat{\Phi}_2$), however, also have a strong effect on the blood pHe (see B).

As shown in the previous section, the sensitivity analysis confirms that none of the variables are sensitive to the parameter representing vascular exchange of the protons between tumour and blood, $\hat{\Gamma}_2$. This suggests that the majority of the removal of protons from the tumour is accomplished via CO_2 evacuation, and not direct movement of free protons. This is reasonable because despite the high proton production of tissues, the actual concentration of free protons in the tissue is very small (several orders of magnitude lower than the respective buffering components). Therefore, by far the majority (ca. ratio of 1 in 10^5) of protons will exit the tumour attached to a buffer.

Unsurprisingly, the parameter incorporating the kinetics of the bicarbonate reaction, $\hat{\alpha}_2$, is shown as important in this analysis, as altering the ratio of the forward to back reactions (and, therefore, the pK_a of the reaction), will strongly alter the effect of the buffer.

The sensitivity of the system with respect to the parameters used for its non-dimensionalisation (for example, δ_1 and δ_3) is not considered, as these parameters do not have a natural biological interpretation. Hence, as initial conditions in the non-dimen-

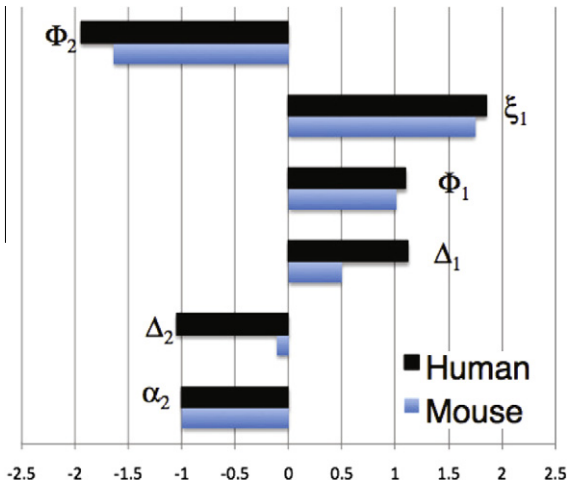

Fig. 7. Tumour H^+ ($\hat{h}_t$) sensitivity coefficients ($S_{h_t,p}$) with respect to parameter (p) with an absolute value greater than 1 for a treated human (black) and mouse (blue). The human tumour pHe is most sensitive to tumour proton production (Φ_2), renal function parameters (ξ_1 and Φ_1), ventilation parameters (Δ_1 and Δ_2), and pK_a (α_2). By comparison, the mouse is less sensitive to the parameters in general, and in particular much less sensitive to the ventilation parameters (Δ_1 and Δ_2). These coefficients were calculated with bicarbonate treatment, values as in Table 1. A table of all the sensitivity coefficients can be found in B. (For interpretation of the references to colours in this figure legend, the reader is referred to the web version of this paper.)

sional system they do not effect the steady state values of the variables.

4. Discussion and conclusion

This paper presents a systemic blood and tumour buffering model, which is parameterised with both mouse and human data sets. The model accurately simulates blood pHe in normal and acid/base disordered states. The simulations indicate that respiratory acidosis and metabolic alkalosis elevate tumor pHe. Conversely, respiratory alkalosis and metabolic acidosis lower tumor pHe to potentially toxic levels. These predictions confirm the hypothesis that inducing metabolic alkalosis through the chronic administration of buffers such as sodium bicarbonate can elevate tumour pHe to normal levels, which has been verified through *in vivo* experiments [11]. This normalisation of tumour pHe could help promote the survival and functions of the normal cells, reducing the tumour's ability to invade. Furthermore, inducing metabolic acidosis is predicted to reduce tumour pHe from the already acidic level, potentially to levels which could be toxic to the tumour cells. Several experimental studies have shown that patients with metastatic renal cancer benefit from cytoreductive nephrectomy [23–25]. Our model supports the speculation by Gatenby and Gawlinski [4] that the observed benefits are a consequence of potential metabolic acidosis caused from the kidney removal, which could lower tumour pHe to levels toxic to the tumour cells.

In order to identify promising proton reducing targets which could prevent tumour acidity and normalise tumour pHe, a sensitivity analysis of the model was performed and indicates that the tumour pHe is most sensitive to tumour proton production and kidney filtration/reabsorption of bicarbonate. For example, the model predicts that decreasing glomerular filtration rate (GFR) leads to a rise in baseline levels of bicarbonate, and any treatment will not be filtered out as effectively. Similarly, the model predicts increasing the renal acid secretion rate would raise bicarbonate levels and significantly increase tumour pHe. However, as treatments targeting these parameters also have a significant effect on blood pHe, any therapy used to adjust kidney function should be undertaken with extreme caution.

On the other hand, altering tumour proton production, $\hat{\Phi}_1$, has a significant effect on tumour pHe, but virtually no effect on blood pHe, and therefore should be considered a safe option. Any potential therapy which could decrease proton production (such as through inhibiting glycolysis) could be used in combination with bicarbonate to an enhanced effect. Ongoing studies by our research group are currently exploring these possibilities.

There are several important extensions to this model which would improve the accuracy of the predictions. First, more detailed modelling of the contribution of other intrinsic buffering components would strengthen the quantitative predictions of the model. The incorporation of these static tissue buffers would not alter the regulation examined in this model, but do contribute to the overall buffering capacity of the tumour. We have assumed a constant buffering contribution from intrinsic buffers, implicitly included in the proton production term. However, it is likely that the intrinsic buffering capacity of the tumour is pH dependent, and thus would be an important model extension to examine. Currently, the model will most likely overestimate the effect of bicarbonate treatment on both the blood and the tissue. Nevertheless, comparing our mathematical model to *in vivo* data indicates this model performs well alone.

Secondly, the predictions in this model are based on the assumption that the tumours in humans will have the same vascularity as in mice, which is not necessarily valid in all cases. However, the cell lines used in the mice were human breast cancer cells, thus it is reasonable to assume the cell lines will produce the same amount of pro-angiogenic signals and therefore initiate similar vasculature. Still, the stromal responses might differ in each situation, which highlights the difficulties of using animal models (even with human cell lines) in therapy experimentation. Additionally, vascular heterogeneity within a single tumour will result in variable buffer delivery across the tumour, which will be important to study with advances in functional vessel imaging.

Thirdly, the effects of systemic alkalosis on respiration is controversial, and we have neglected the effect of H^+ on ventilation rate for several reasons. Firstly, isolated changes in H^+ are mainly sensed by the peripheral chemoreceptors [26], which only contribute a small amount to ventilation. Secondly, respiratory compensation to metabolic alkalosis is controversial [27–29]. Early studies indicated that there was little to no respiratory compensation in humans and dogs [27,28]. Later studies have shown that in some human cases there is respiratory compensation, although the magnitude of compensation is highly variable, and in all cases limited [30]. Even in cases of severe metabolic alkalosis, it is extremely rare to see respiratory compensation raising pCO_2 levels above 55 mm Hg from the normal 40 mm Hg [31,32]. There is no concrete evidence surrounding murine respiratory compensation. However, respiratory compensation to metabolic alkalosis is present in some humans. As our model system is sensitive to the ventilation term, the refinement of this term is worth further consideration.

Experimental studies undertaken by our group are currently examining the presence (or absence) of respiratory compensation in mice, which will hopefully elucidate the variability, timing, and extent of this compensation should it occur. These and other experimental results will be used to refine and develop the current model, which can further aid in developing safe and effective anti-tumour therapies.

Despite the many possible extensions, our simplified model accurately predicts acid–base regulation in the blood and tumour, and can be used to suggest the most promising parameters and processes to target in order to reduce tumour acidity and prolong survival. Novel therapies utilising exogenous buffers or other combinations can be built on this basic framework for future study. Finally, this model could be linked to other cellular models of tumour growth [33,34], and subcellular models of tumour metab-

olism to provide a multiscale model linking pHe regulation with tumour invasion.

Acknowledgments

Grant Support NKM: This publication was funded by the National Cancer Institute, NIH grant U56CA113004. PKM: This work was partially supported by a Royal Society-Wolfson Research Merit Award. RAG and PKM: This work was partially supported by NIH grant 1U54CA143970-01. RJG and IR: This work was supported by NIH grant R01 CA 077575.

Appendices A and B Supplementary data

Supplementary data associated with this article can be found, in the online version, at doi:10.1016/j.mbs.2010.12.002.

References

[1] R. Gatenby, R. Gillies, Why do cancers have high aerobic glycolysis?, Nat Rev. Cancer 4 (11) (2004) 891.
[2] R. Gillies, I. Robey, R. Gatenby, Causes and consequences of increased glucose metabolism of cancers, J. Nucl. Med. 49 (Suppl. 2) (2008) 24S.
[3] O. Warburg, On the origin of cancer cells, Science 123 (3191) (1956) 309.
[4] R. Gatenby, E. Gawlinski, The glycolytic phenotype in carcinogenesis and tumor invasion: insights through mathematical models, Cancer Res. 63 (14) (2003) 3847.
[5] G. Helmlinger, F. Yuan, M. Dellian, R. Jain, Interstitial pH and pO_2 gradients in solid tumors in vivo: high-resolution measurements reveal a lack of correlation, Nat. Med. 3 (2) (1997) 177.
[6] P. Schornack, R. Gillies, Contributions of cell metabolism and H^+ diffusion to the acidic pH of tumors, Neoplasia 5 (2) (2003) 135.
[7] I. Tannock, D. Rotin, Acid pH in tumors and its potential for therapeutic exploitation, Cancer Res. 49 (16) (1989) 4373.
[8] R. Gatenby, E. Gawlinski, A reaction–diffusion model of cancer invasion, Cancer Res. 56 (24) (1996) 5745.
[9] R. Gatenby, E. Gawlinski, A. Gmitro, B. Kaylor, R. Gillies, Acid-mediated tumor invasion: a multidisciplinary study, Cancer Res. 66 (10) (2006) 5216.
[10] R. Gatenby, R. Gillies, Glycolysis in cancer: a potential target for therapy, Int. J. Biochem. Cell Biol. 39 (7–8) (2007) 1358.
[11] I. Robey, B. Baggett, N. Kirkpatrick, D. Roe, J. Dosescu, B. Sloane, A. Hashim, D. Morse, N. Raghunand, R. Gatenby, R. Gillies, Bicarbonate increases tumor pH and inhibits spontaneous metastases, Cancer Res. 69 (6) (2009) 2260.
[12] A. Silva, J. Yunes, R. Gillies, R. Gatenby, The potential role of systemic buffers in reducing intratumoral extracellular pH and acid-mediated invasion, Cancer Res. 69 (6) (2009) 2677.
[13] C. Chegwidden, E. Edwards, The Carbonic Anhydrases: New Horizons, Birkhauser, 2000.
[14] K. Nordfors, J. Haapasalo, M. Korja, A. Niemela, J. Laine, A. Parkkila, S. Pastorekova, J. Pastorek, A. Waheed, W. Sly, S. Parkkila, H. Haapasalo, Biochemical characterization of CA IX, one of the most active carbonic anhydrase isozymes, BMC Cancer 10 (2008) 27799.
[15] M. Hilvo, L. Baranauskiene, A. Salzano, A. Scaloni, D. Matulis, A. Innocenti, A. Scozzafava, S. Monti, A. DiFiore, G. DeSimone, M. Lindfors, J. Janis, J. Valjakka, S. Pastorekova, J. Pastorek, M. Kulomaa, H. Nordlund, C. Supuran, S. Parkkila, Biochemical characterization of CA IX, one of the most active carbonic anhydrase isozymes, J. Biol. Chem. 283 (2008) 27799.
[16] R. Jain, Transport of molecules across tumor vasculature, Cancer Metastasis Rev. 6 (4) (1987) 559.
[17] R. Hainsworth, Acid–Base Balance, Manchester University, 1986.
[18] H. Davenport, The ABC of Acid–Base Chemistry, The University of Chicago, 1974.
[19] J. Widdicombe, A. Davies, Respiratory Physiology, Edward Arnold Publishers, 1983.
[20] R. Mitchell, M. Singer, Respiration and cerebrospinal fluid pH in metabolic acidosis and alkalosis, J. Appl. Physiol. 20 (1965) 905.
[21] V. Fencl, J. Vale, J. Broch, Respiration and cerebral blood flow in metabolic acidosis and alkalosis in humans, J. Appl. Physiol. 27 (1969) 67.
[22] W. Yee, E. Scarpelli, CO_2 responsivity in the mouse measured by rebreathing, Pflugers Archives 406 (6) (1986) 615.
[23] J. Montie, B. Stewart, R. Straffon, C. Hewitt, D. Montague, The role of adjunctive nephrectomy in patients with metastatic renal cancer, J. Urol. 97 (1967) 973.
[24] S. Marcus, P. Choyke, R. Reither, G. Jaffe, R. Alexander, W. Lineham, S. Rosenberg, M. Walther, Regression of metastatic renal cell carcinoma after cytoreductive nephrectomy, J. Urol. 150 (1993) 463.
[25] G. Mickisch, A. Garin, H. van Poppel, L. de Prijck, R. Sylvester, Radical nephrectomy plus interferon-alfa-based immunotherapy compared with interferon-alfa alone in metastatic renal carcinoma. A randomized trial, Lancet 358 (2001) 948.
[26] M. Levitzky, Pulmonary Physiology, McGraw-Hill Book Co., 2003.
[27] K. Roberts, J. Poppell, P. Vanamee, R. Beals, H. Randall, Evaluation of respiratory compensation in metabolic alkalosis, J. Clin. Invest. 35 (2) (1956) 261.
[28] J. Poppell, P. Vanamee, K. Roberts, H. Randall, The effect of ventilatory insufficiency on respiratory compensations in metabolic acidosis and alkalosis, J. Lab. Clin. Med. 47 (6) (1956) 885.
[29] J. Ward, J. Ward, C. Wiener, R. Leach, The Respiratory System at a Glance, Blackwell Science, 2002.
[30] S. Javaheri, N.S. Shore, B. Rose, H. Kazemi, Compensatory hypoventilation in metabolic alkalosis, Chest 81 (3) (1982) 296.
[31] D. Hornick, An Approach to the Analysis of Arterial Blood Gases and Acid–Base Disorders, Virtual Hospital, University of Iowa Health Care [On-line], 2003.
[32] J. Feldman, L. Zimmerman, Introduction to Arterial Blood Gases, Part 2, 2001. Available from: <http://missinglink.ucsf.edu/lm/abg/abg2/compensation.html>.
[33] K. Smallbone, R. Gatenby, R. Gillies, P. Maini, D. Gavaghan, Metabolic changes during carcinogenesis: potential impact on invasiveness, J. Theor. Biol. 244 (4) (2007) 703.
[34] T. Alarcon, M. Owen, H. Byrne, P. Maini, Multiscale modelling of tumour growth and therapy: the influence of vessel normalisation on chemotherapy, Comp. Math. Meth. Med. 7 (2006) 85.
[35] E. Green, Biology of the Laboratory Mouse, Dover Publications, 1966.
[36] The Jackson Laboratory, Mouse Tumor Biology Database, 2009. Available from: <http://tumor.informatics.jax.org>.
[37] R. Jain, Delivery of molecular and cellular medicine to tumors, Tumor Pathophysiol. Transp. Phenom. Course Notes (2005) 55.
[38] V. Endeward, Low carbon dioxide permeability of the apical epithelial membrane of guinea-pig colon, J. Physiol. Lond. 567 (1) (2005) 253.
[39] G. Cooper, W. Boron, Effect of PCMBS on CO_2 permeability of Xenopus oocytes expressing aquaporin 1 or its C189S mutant, Am. J. Physiol. Cell Physiol. 275 (1998) 1481.
[40] W. Monsky, C. Carreira, Y. Tsuzuki, T. Gohongi, Role of host microenvironment in angiogenesis and microvascular functions in human breast cancer xenografts: mammary fat pad versus cranial tumors, Clin. Cancer Res. 8 (2002) 1008.
[41] J. Missbach-Guentner, C. Dullin, S. Kimmina, M. Zientkowska, M. Domeyer-Missbach, C. Malz, E. Grabbe, W. Stühmer, F. Alves, Morphologic changes of mammary carcinomas in mice over time as monitored by flat-panel detector volume computed tomography, Neoplasia 10 (7) (2008) 663.
[42] M. Gee, W. Procopio, S. Makonnen, M. Feldman, N. Yeilding, W. Lee, Tumor vessel development and maturation impose limits on the effectiveness of anti-vascular therapy, Am. J. Pathol. 162 (1) (2003) 183.
[43] M. Dadiani, R. Margalit, N. Sela, H. Degani, High-resolution magnetic resonance imaging of disparities in the transcapillary transfer rates in orthotopically inoculated invasive breast tumors, Cancer Res. 64 (2004) 3155.
[44] S. Singletary, C. Allred, P. Ashley, L. Bassett, D. Berry, K. Bland, P. Borgen, G. Clark, S. Edge, D. Hayes, Revision of the American Joint Committee on cancer staging system for breast cancer, J. Clin. Oncol. 20 (2002) 3628.
[45] G. Martin, R. Jain, Noninvasive measurement of interstitial pH profiles in normal and neoplastic tissue using fluorescence ratio imaging microscopy, Cancer Res. 54 (21) (1994) 5670.
[46] M. Mackey, L. Glass, Oscillation and chaos in physiological control systems, Science 197 (4300) (1977) 287.
[47] R. Chambrey, D. Goossens, S. Bourgeois, N. Picard, M. Bloch-Faure, F. Leviel, V. Geoffroy, M. Cambillau, Y. Colin, M. Paillard, P. Houillier, J. Cartron, D. Eladari, Genetic ablation of Rhbg in the mouse does not impair renal ammonium excretion, Am. J. Physiol. Renal Physiol. 289 (6) (2005) F1281.
[48] P. Meneton, I. Ichikawa, T. Inagami, J. Schnermann, Renal physiology of the mouse, Am. J. Physiol. Renal Physiol. 278 (3) (2000) F339.
[49] D. Levine, M. Iacovitti, S. Robertson, Modulation of single nephron GFR in the db/db mouse model of Type 2 Diabetes Mellitus. II. Effects, Am. J. Physiol. Reg. Integ. Comp. Physiol. 294 (2008) 1840.
[50] R. Pitts, Physiology of the Kidney and Body Fluids, Year Book Medical Publishers Inc, 1970.
[51] A. Vander, Renal Physiology, McGraw-Hill Book Co., 2004.
[52] C. Lote, Principles of Renal Physiology, Kluwer Academic Publishers, 1999.
[53] S. Wetterlin, C. Pettersson, Determination of cardiac output in the mouse, Res. Exp. Med. 174 (1979) 143.
[54] R. Putnam, A. Roos, Which value for the first dissociation constant of carbonic acid should be used in biological work?, Am J. Physiol. Cell Physiol. 260 (1991) C1113.
[55] E. Freireich, E. Gehan, D. Rall, L. Schmidt, Quantitative comparison of toxicity of anticancer agents in mouse, rat, hamster, dog, monkey and man, Cancer Chemother. Rep. 50 (4) (1966) 219.
[56] D. Krupke, D. Begley, J. Sundberg, C. Bult, J. Eppig, The mouse tumor biology database, Nat. Rev. Cancer 8 (6) (2008) 459.
[57] R. Jain, Transport of molecules in the tumor interstitium: a review, Cancer Res. 47 (1987) 3039.
[58] F. Han, S. Subramanian, E. Price, J. Nadeau, K. Strohl, Periodic breathing in the mouse, J. Appl. Physiol. 92 (3) (2002) 1133.
[59] D. Oken, An analysis of glomerular dynamics in rat, dog, and man, Kidney Int. 22 (1982) 136.